An Adaptive Thunderstorm Measurement Concept Using C-Band and X-Band Radar Data

Jacopo Grazioli, Andreas Leuenberger, Lionel Peyraud, Jordi Figueras i Ventura, Marco Gabella, Alessandro Hering, and Urs Germann

***Abstract*— This letter presents a proof of concept illustrating the possibility to integrate X-band radar scans of individual thunderstorm cells within an operational context of storm cells identification, tracking, and severity ranking performed by a long-range volume-scanning surveillance C-band radar network. The X-band radar performs adaptive 3-D scans of one automatically selected cell, i.e., the most intense storm cell within its domain, previously identified by the operational C-band radars. The scan aims to observe with high spatiotemporal resolution the core of the cell and the evolution of its vertical structure, providing a unique data set for microphysical and dynamical interpretations. The cells tracked with this method by the X-band radar can be characterized with a high spatiotemporal resolution, better with respect to the operational C-band measurements, as illustrated in the letter with a case study of a supercellular storm occurring in western Switzerland on June 7, 2015. This method is a valuable example of the potential added value of an X-band radar system of flexible scanning strategy, in addition to C-band operational measurements conducted with a fixed scanning protocol.**

***Index Terms*— Polarimetric weather radar, storm tracking, thunderstorm, X-band.**

I. Introduction

OPERATIONAL weather agencies usually deploy a network of C-band and S-band weather radars to quantify and monitor precipitation with the necessary redundancy over the scale of a country [1]. At these radar frequencies, the attenuation of the radar signal by precipitation is often of minor importance, and therefore, long-range monitoring is achieved with a small number of radar installation sites. In regions of complex topography, for example, Switzerland, the operational radar systems are installed in elevated sites, in order to maximize long-range visibility [2]. As a tradeoff, the radar beams are often crossing the atmosphere hundreds or thousands of meters above ground over narrow Alpine valleys, thus leaving "blind" areas extending from the height of the beam down to the surface. Extrapolations at the ground level, therefore, need an appropriate correction of the vertical profiles [3], while the local variations of the vertical structure of precipitation may be lost. Operational weather radar monitoring in Switzerland is conducted by means of 5 C-band dual-polarization Doppler radars. Each radar performs a volume scan consisting of 20 interleaved elevations between $-0.2°$ and $40°$, with 5-min repetition time. As in most operational radar networks, robustness, reliability, and continuous nation-wide 24/7 surveillance requirements dictate that the scanning strategy of each radar is fixed and does not adapt in response to current weather. Adaptive scanning is an important research topic [4], especially given the rising of phased-array radar technologies that could ease its implementation, but it is still not largely applied for operational monitoring worldwide.

Mobile X-band weather radar systems have been proven useful for scientific field campaigns devoted to the observation of precipitation microphysics, also in complex terrains and narrow Alpine valleys [5], [6]. Being frequently used for dedicated campaigns, they often do not remain for long in the same location and are not integrated with operational radar composites. In some cases, however, X-band weather radars are used operationally, either as short-range "gap fillers" for radar composites [7] or for urban-scale high-resolution monitoring, given their lower cost, size, power consumption, and reduced installation logistic requirements [1], [8], [9]. The first relevant efforts have also been recently conducted toward the operational use of X-band radar in a network [10] operating with an adaptive scanning approach.

In this letter, we describe an approach, developed at MeteoSwiss, to make synergetic use of operational weather radar products (C-band), and data from a mobile X-band system in order to obtain high-resolution measurements of intense thunderstorm cells and maximize the benefits of the different characteristics of the two systems. The C-band radars follow a fixed scanning sequence and provide a large-scale overview, while the X-band radar adapts dynamically its scanning protocol in reaction to the presence, within its domain, of interesting storm cells.

The manuscript is structured as follows. Section II presents the operational radar-based monitoring of thunderstorm cells and the novel X-band adaptive scan. Section III provides an example of a particularly interesting storm case. Section IV draws the main conclusions and perspectives of the method.

II. Thunderstorm Cells Observations at C-Band and X-Band

A. C-Band Thunderstorm Radar Tracking

MeteoSwiss developed an operational nowcasting tool, the Thunderstorms Radar Tracking (TRT hereafter) [11]–[13],

Manuscript received January 16, 2019; revised March 25, 2019; accepted March 30, 2019. Date of publication June 21, 2019; date of current version October 30, 2019. *(Corresponding author: Jacopo Grazioli.)*

The authors are with the Swiss Federal Office of Meteorology and Climatology, MeteoSwiss, CH-6605 Locarno-Monti, Switzerland (e-mail: jacopo.grazioli@meteoswiss.ch).

This article has supplementary downloadable material available at http://ieeexplore.ieee.org, provided by the author.

Color versions of one or more of the figures in this letter are available online at http://ieeexplore.ieee.org.

Digital Object Identifier 10.1109/LGRS.2019.2909970

to track, rank, and predict the displacement of thunderstorm cells throughout their life cycle. The tool is based on 3-D reflectivity data collected by five C-band radars of the operational network. A dynamic threshold scheme is employed in order to adapt the algorithm to the development stage of individual storm cells. The identified cells are ranked every 5 min with a numerical severity score ranging from 0 to 40, corresponding to five main categories: very weak (0–12), weak (12–25), moderate (15–25), severe (25–35), and very severe (35–40). The ranking results from a combination of mean echo top height at 45 dBZ, maximum reflectivity, vertically integrated liquid water content, and the storm area $\geq$57 dBZ (see [13]). TRT cells are identified without assuming *a priori* a given shape, and for further operational use, to help the forecasters to issue alerts based on 2-D maps, they are approximated with an elliptic shape. The ellipse is fully parametrized by its centroid, minor axis, major axis, and orientation, and it has the same area of the original cell. Apart from operational alert decisions, the TRT tool has been proven useful to describe and characterize intense hail-bearing storms, thanks to the large available historical data set (e. g., [12], [13]).

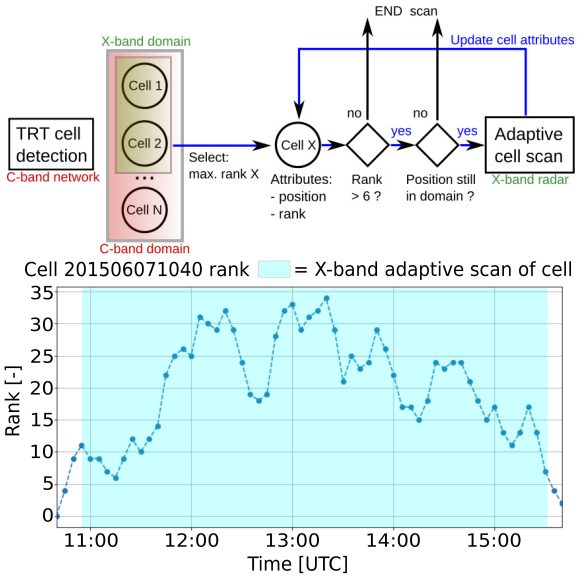

Fig. 1. (Top) Flowchart illustrating the main concept of the adaptive X-band cell scan in response to the operational TRT product. (Bottom) Example of rank evolution with time of a cell within the X-band domain and tracked by the TRT from 1040 UTC on June 7, 2015. Highlighted in light blue are the time steps where the cell was targeted by the adaptive X-band scan (1055–1530 UTC).

B. X-Band Integration

MeteoSwiss also operates an X-band dual-polarization Doppler weather radar. The radar is a mobile Meteor 50DX manufactured by Selex-Gematronik, and it is employed mostly for project-based measurement campaigns outside the operational network. It can be easily transported from site to site, although it is not conceived to perform measurements during its transport. It collects the most common polarimetric variables: horizontal (vertical) reflectivity Z_H (Z_V), differential reflectivity Z_{DR}, copolar correlation coefficient ρ_{HV}, total differential phase shift Ψ_{dp}, specific differential phase shift K_{dp}, Doppler velocity, and Doppler spectrum width. Other derived quantities, for example, hydrometeor classification [14], [15], useful to perform microphysical characterization of storm cells [16], are also computed. Unlike the operational C-band radars, this system: 1) is often deployed in the valleys and its lowest beams are closer to the ground; 2) can perform genuine Range-Height Indicator (RHI) scans; and 3) is not bound to a given scanning strategy dictated by operational needs, except for exceptional measurement periods. The idea presented in this letter involves the integration of this system into the existing TRT framework by taking advantage of its flexibility to follow an adaptive scanning sequences. The integration principle is summarized in Fig. 1 (top).

During normal operation, a background software constantly monitors the eventual presence of cells identified by the TRT in the measurement domain of the 50DX. This measurement domain is defined by a minimum radius, centered at the radar site. If one or more cells are found, the one with the highest severity rank is selected and its geographical information is sent to the 50DX controller. The 50DX immediately interrupts its current scanning strategy and activates a dedicated scan triggered by the presence of the TRT cell: it performs one RHI scan toward the position of the cell center (defined by the centroid of the ellipse), two RHIs, respectively, at $\pm 1^\circ$ of azimuth with respect to the center, and a Plan Position Indicator (PPI) scan at a low elevation angle to provide larger scale view. The scan is repeated with a cycling time of 1.5 min and it is updated when the operational TRT information updates the position of the cell every 5 min. An overview of the adaptive sequence capturing the 3-D structure of a storm with its PPI and RHIs scans is shown in Fig. 2, taking as an example the variables of horizontal reflectivity Z_H and Doppler velocity. For this type of scan, the maximum range covered by the X-band radar is 60 km, with and unambiguous Doppler velocity of $\pm 47\ \mathrm{ms}^{-1}$.

Once a cell is tracked, the adaptive scanning strategy is repeated for as long as the cell remains in the measurement domain or its severity level goes below a predefined severity rank. The global behavior of the 50DX adaptive scan is controlled by a set of editable parameters. An example of the main parameters of this set is given in Table I. The number of RHIs and their azimuthal direction with respect to the cell core can be selected, as well as their coverage in elevation, following the idea that the closer the cell is with respect to the radar, the larger the elevation span must be in order to capture its full vertical extension.

This adaptive scan is a valid example of possible automatic integration, in reaction to the current weather situation, of an X-band system within an operational network of C-band radars. Cells are observed by means of genuine RHIs, thus improving dramatically the quality of observation of the vertical structure of the storms, as it will be shown in Section III. Being focused on one individual cell, the scan can also achieve a high temporal resolution. Since 2014, the integration of the TRT into X-band measurements was tested for two different X-band radar sites in Switzerland.

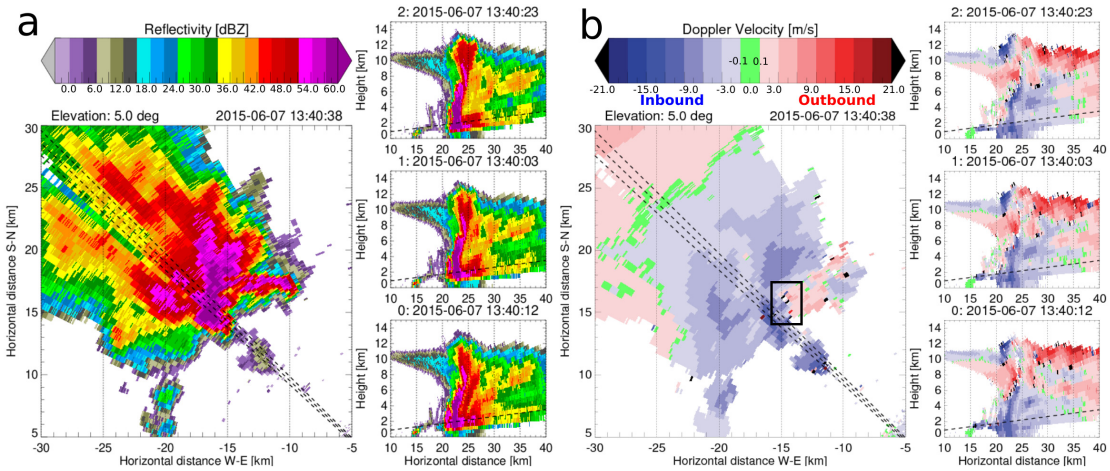

Fig. 2. (a) Example of adaptive scan X-band images (PPI + 3 RHIs) of horizontal reflectivity Z_H. (b) Doppler velocity of the cell tracked on June 7, 2015 (see Figs. 1 and 3) during one of the most intense timesteps. Horizontal distances on the graphs are referred with respect to the X-band radar location. A rectangle on (b) is used to highlight an area where rotational couplets are observed.

TABLE I

EXAMPLE OF THE MAIN SETUP PARAMETERS FOR THE INTEGRATION OF THE X-BAND MEASUREMENTS IN THE OPERATIONAL TRT CONTEXT

Parameter	Explanation	Units	Example value
RADAR_LAT	X-band radar latitude	°	46.84249
RADAR_LON	X-band radar longitude	°	6.91836
RADAR_ALT	X-band radar altitude	m.a.s.l	450
TRT_MIN_RANK_START	Minimum cell rank to trigger X-band adaptive scan	-	10
TRT_MIN_RANK_STOP	Minimum cell rank to stop X-band adaptive scan	-	6
RADAR_MIN_DIST_START	Minimum distance of cell core with respect to X-band radar before to start X-band scan	km	50
RADAR_MIN_DIST_STOP	Minimum distance of cell core with respect to X-band radar before to stop X-band scan	km	60
PPI_ANGLE	Elevation angle of the PPI in the X-band scan	°	4
RHI_NUM	Number of RHI scans	-	3
AZ_OFFSET_0,1,2	Offset in azimuth with respect to cell core towards where to conduct the first (second, third) RHI scan	°	0, 1, -1
ELMAX_NUM	Number of adaptive maximum elevation angles of RHI scans	-	3
ELMAX_RANGE_0,1,2	Range distance thresholds defining adaptive maximum elevation angles.	km	25, 15, 5
ELMAX_0,1,2,3	Adaptive maximum elevation angles according to distance thresholds.	°	40, 60, 90, 180

The X-band adaptive scan has been triggered during 79 days, for 320 cells fulfilling the tracking conditions while they were within the X-band measurement domain.

C. Requirements, Limitations, and Improvements

The adaptive scan of individual thunderstorm cells is undoubtedly an added value to the operational scans, but in order to perform efficiently it requires at least: 1) direct real-time communication between the mobile system and the TRT operational output; 2) a mobile system that can be easily controlled by automatic scripting. The approach, as presented here, has some current limitations that leave space for improvements or adaptations. Initially, the cell with the highest TRT rank is always selected and scanned, once it enters the measurement domain. This cell may or may not be the most interesting one from a meteorological viewpoint during its entire life cycle. Other cells of lower initial rank (thus not selected for the adaptive scan) can evolve and increase their intensity or may cross more sensitive populated areas. Second, the position of the thunderstorm cells is updated using TRT information only (every 5 min). A future version of the technique is currently being investigated where the X-Band radar would perform independent cell identification and tracking using the C-band based TRT only as initialization, in order to fully exploit the higher temporal resolution available with the X-band adaptive scans. In addition, the current conditions allowing a cell to be tracked do not consider the actual visibility of the X-band radar over the cell itself, mainly due to the surrounding topographic obstacles. Finally, while the technique is integrated into the operational TRT process, it is not currently operational and remains at the stage of proof of concept. Given the high resolution of the measurements, and the better low-level visibility gained on the cells themselves, such an approach has the potential to be used to improve the operational response to localized severe thunderstorms, also from a nowcasting point of view.

III. Example of Application: June 7, 2015

The beginning of June 2015 was a favorable period for the development of strong to severe thunderstorms over Switzerland [13]. On June 7, 2015, the X-band weather radar was deployed in Payerne (CH), close to the southern shore of Lake Neuchâtel (exact position as indicated in Table I). At about 1100 UTC, until about 1430 UTC, a high-intensity TRT cell entered the measurement domain of the X-band radar, triggering the dedicated X-band scan. The cell moved from southwest to northeast, north of Lake Neuchâtel into the region of the Swiss Jura, in an area where the X-band radar had good visibility and could sample the cell with its RHIs from ground level to cloud top. During its life cycle, the cell developed supercell features and produced a short-lived tornado. These thunderstorm structures occasionally occur in Switzerland, as described in [17]. According to video-supported reports, the tornado reached the ground at about 1340 UTC. Radar images of the tornado, at about the time of touchdown, are shown in Fig. 2, which depicts the 3-D storm structure by showing the PPI and the RHIs of one cycle of the adaptive scan sequence. Z_H values were larger than 60 dBZ in the core of the storm, and the effect of signal attenuation is evident behind it, partially mitigated by the attenuation correction applied [18]. An indication of a rotational couplet can be observed in the Doppler velocity measurements of Fig. 2 (b) The atmospheric sounding of Payerne at 12 UTC (roughly the same location as the X-band radar site) showed a high CAPE of 1565 Jkg^{-1}, and relatively low wind shear: conditions more favorable to multicellular storm clusters rather than supercellular development. However, the low-level northeasterly "Bise" wind on the order of 10–15 kts (5–8 ms^{-1}), in combination with the 500-hPa southwesterly wind on the order of 15 kts and the inflow of the storm, most likely allowed the cell to develop supercellular features during a portion of its lifecycle (Lionel Peyraud, personal communication). Fig. 3 shows the trajectory of the identified cell center, from 11 UTC to 1530 UTC, together with the location of hail reports provided through the MeteoSwiss mobile application [13]. Hail was reported from 13 UTC to 1430 UTC, corresponding to the timestep of particularly intense vertical development.

For this fast-evolving cell with a complex structure, the high-resolution 3-D measurements of the X-band radar allowed complementing the C-band measurements, providing a better sample of the vertical structure of the system. Fig. 4 shows median values of reflectivity Z_H within the cell, as a function of altitude and time, as seen by the RHI scans of the 50DX radar toward the core of the thunderstorm cell. Although this is a way to largely summarize the 3D+time structure of the cell into one individual image, several features are also evident in this simplified representation, and similar high-resolution reconstructions are not achievable with the data of the operational volume scans of the C-band radars. The most intense development of the cell is observed between 1230 UTC and 1330 UTC, with the second peak of intensity at about 1430 UTC, corresponding roughly to the times when the hail was observed. The echo top height, accurately displayed, thanks to the genuine RHI scans, is located at approximately 14 km meters above sea level during the most intense phases

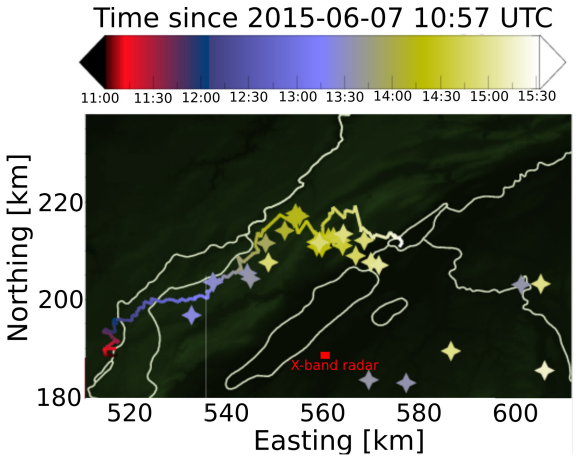

Fig. 3. Trajectory of the storm cell shown in Fig. 1, color-coded according to the time elapsed since the beginning of the X-band adaptive scan. Individual symbols on the map (as well color-coded) locate the position and time of crowdsourcing hail reports from the users of the MeteoSwiss mobile application. Coordinates on the map are in the Swiss Coordinate system CH1903 / LV03 (https://www.swisstopo.admin.ch/en/knowledge-facts/surveying-geodesy/reference-systems/map-projections.html). The location of the X-band radar is indicated on the map. The closest C-band radar of "La Dôle" is located at coordinates 497.1 E, 142.4 N, out of the domain covered in this image.

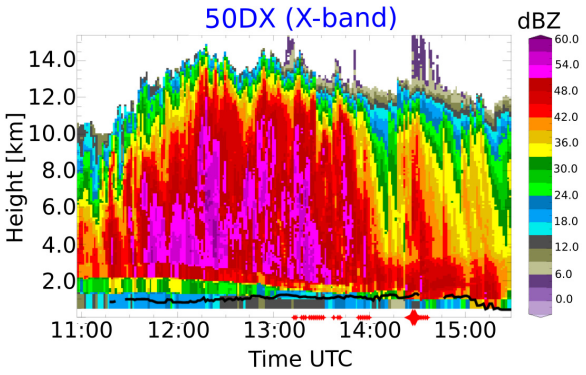

Fig. 4. Time–height evolution of Z_H (dBZ) within an individual storm cell identified on June 7, 2015. The data shown come from the adaptive scan of the X-band radar. For each height level, the 50% quantile of Z_H within the cell core, from genuine RHIs is shown. A solid black line indicates the altitude of the terrain, and individual red symbols are used to mark the occurrence of hail in the surrounding of the cell, provided by user reports through the MeteoSwiss mobile application.

of the storm. The presence of hail as dominant hydrometeor close to the ground level is also observed in the hydrometeor classification data (Fig. 5), as well as a large presence of graupel in the ice-phase portion of the storm. The level of detail of the vertical structure is significantly better captured by the X-band radar with respect to what could be inferred from volume scans of the C-band radars, thanks to: 1) genuine RHIs; 2) better temporal resolution of the scanning sequence; and 3) proximity to the cell. In this context, X-band data are complementary information to improve the observations of thunderstorms along the vertical dimension and with higher temporal sampling, within a domain scale $\leq$100 km. This added value may, therefore, be relevant for individual cities, airports, or sensitive events. A few animations of this case

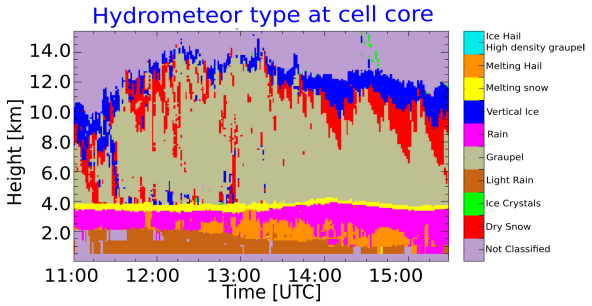

Fig. 5. As Fig. 4, but showing the time–height evolution of hydrometeor classification. The classification method of [15] is used, and the most represented hydrometeor type for each height level (mode) is shown.

study are also provided as supplementary material, to better illustrate the principle of the adaptive scan and the type of data that it can provide.

IV. Conclusion

With this letter, we presented a proof of concept of integration of X-band radar data to improve the 3-D sampling of intense storm cells previously identified by an operational algorithm based on C-band operational weather radars. Although the C-band radars perform their standard scanning sequence, the X-band radar is left free to perform adaptive scans of the most intense cell within its domain, with high spatiotemporal resolution and improved vertical representation thanks to genuine RHI scans and to the deployment site of the X-band radars, often located at a much lower altitude than the otherwise lowest available C-band radar elevation scan in the complex orography of Switzerland. We demonstrated the added value of such measurements with an example of a very intense, hail-bearing cell occurring in June 2015 in Western Switzerland. High-resolution data of individual storm cells can be compiled thanks to this strategy, with the current tradeoff being that only one cell can be tracked at once among the ones entering the radar domain. The implementation requires real-time communication between the X-band system and the C-band radars, and it requires the X-band radar to be fully flexible to operate adaptive scans. The potential side benefits of such set-ups include: 1) improved quantitative precipitation estimation (QPE) inside mountain valleys, following a strategic installation of X-band radars; 2) analysis of microphysical mechanisms characterizing storm cells through their life cycle; 3) improved short-term representation of thunderstorms; and 4) unprecedented data for a better understanding of storm dynamics and microphysics. Although the method is only a particular example of an application of an X-band radar in an operational context and it is currently a proof of concept, it represents a step forward toward the more frequent use of weather-dependent adaptive scans, which currently still remain largely underused in an operational context. Such a scenario can make particular sense in regions of enhanced interest, such as a city, an airport or a big sports event, where an X-band radar integrated into a C-band network could be allowed to focus on the most intense storms the task of large-scale monitoring to the C-band network.

Acknowledgment

The authors would like to thank M. Schneebeli and S. Joos, who managed the X-band radar system, where several cell measurements were conducted, for the period 2015–2016.

References

[1] D. Zrnic, "S, C, and X bands for weather surveillance," NOAA Nat. Severe Storms Lab., Washington, DC, USA, Tech. Rep., 2017. [Online]. Available: https://www.google.ch/url?sa=t&rct=j&q=&esrc=s&source=web&cd=1&ved=2ahUKEwiEtv6-4ejiAhWjxoUKHRmZCtAQFjAAegQIABAC&url=https%3A%2F%2Fwww.nssl.noaa.gov%2Fpublications%2Fmpar_reports%2FS-C-X%2520Bands%2520for%2520Weather%2520SurveillFINAL.docx%3Fv%3D02may2017&usg=AOvVaw0N2zz-Q1hVsChja1ODGXZH

[2] U. Germann, M. Boscacci, M. Gabella, and M. Sartori, "Radar design for prediction in the Swiss alps," *Meteorol. Technol. Int.*, no. 4, pp. 42–45, Apr. 2015.

[3] U. Germann and J. Joss, "Mesobeta profiles to extrapolate radar precipitation measurements above the Alps to the ground level," *J. Appl. Meteorol.*, vol. 41, no. 5, pp. 542–557, May 2002.

[4] R. L. Tanamachi and P. L. Heinselman, "Rapid-scan, polarimetric observations of central Oklahoma severe storms on 31 May 2013," *Weather Forecast.*, vol. 31, no. 1, pp. 19–42, Feb. 2016.

[5] M. Schneebeli, N. Dawes, M. Lehning, and A. Berne, "High-resolution vertical profiles of polarimetric X-band weather radar observables during snowfall in the Swiss Alps," *J. Appl. Meteorol. Clim.*, vol. 52, no. 2, pp. 378–394, Feb. 2013.

[6] J. Grazioli *et al.*, "Polarimetric radar and *in situ* observations of riming and snowfall microphysics during CLACE 2014," *Atmos. Chem. Phys.*, vol. 15, no. 23, pp. 13787–13802, 2015. [Online]. Available: https://www.atmos-chem-phys.net/15/13787/2015/

[7] J. F. I. Ventura and P. Tabary, "The new French operational polarimetric radar rainfall rate product," *J. Appl. Meteorol. Climatol.*, vol. 52, no. 8, pp. 1817–1835, Aug. 2013.

[8] F. Junyent, V. Chandrasekar, D. McLaughlin, E. Insanic, and N. Bharadwaj, "The CASA integrated project 1 networked radar system," *J. Atmos. Ocean. Technol.*, vol. 27, no. 1, pp. 61–78, 2010.

[9] H. Chen and V. Chandrasekar, "The quantitative precipitation estimation system for Dallas–Fort Worth (DFW) urban remote sensing network," *J. Hydrol.*, vol. 531, pp. 259–271, Dec. 2015.

[10] V. Chandrasekar, H. Chen, and B. Philips, "Principles of high-resolution radar network for hazard mitigation and disaster management in an urban environment," *J. Meteorolog. Soc. Jpn.*, vol. 96, pp. 119–139, Jan. 2018.

[11] A. M. Hering, C. Morel, G. Galli, S. Sénési, P. Ambrosetti, and M. Boscacci, "Nowcasting thunderstorms in the alpine region using a radar based adaptive thresholding scheme," in *Proc. 3rd Eur. Conf. Radar Meteorol. Hydrol.*, Visby, Sweden, Sep. 2004, pp. 206–211.

[12] L. Nisi, A. Hering, U. Germann, and O. Martius, "A 15-year hail streak climatology for the Alpine region," *Quart. J. Roy. Meteorolog. Soc.*, vol. 144, no. 714, pp. 1429–1449, Jul. 2018.

[13] S. Trefalt *et al.*, "A severe hail storm in complex topography in Switzerland—Observations and processes," *Atmos. Res.*, vol. 209, pp. 76–94, Sep. 2018.

[14] J. Grazioli, D. Tuia, and A. Berne, "Hydrometeor classification from polarimetric radar measurements: A clustering approach," *Atmos. Meas. Techn.*, vol. 8, no. 1, pp. 149–170, 2015.

[15] N. Besic, J. Grazioli, M. Gabella, U. Germann, and A. Berne, "Hydrometeor classification through statistical clustering of polarimetric radar measurements: A semi-supervised approach," *Atmos. Meas. Techn.*, vol. 9, no. 9, pp. 4425–4445, Sep. 2016. [Online]. Available: https://www.atmos-meas-tech.net/9/4425/2016/

[16] A. V. Ryzhkov, T. J. Schuur, D. W. Burgess, P. L. Heinselman, S. E. Giangrande, and D. S. Zrnic, "The joint polarization experiment: Polarimetric rainfall measurements and hydrometeor classification," *Bull. Amer. Meteorolog. Soc.*, vol. 86, no. 6, pp. 809–824, Jun. 2005.

[17] L. Peyraud, "Analysis of the 18 July 2005 tornadic supercell over the lake geneva region," *Weather Forecast.*, vol. 28, no. 6, pp. 1524–1551, Dec. 2013.

[18] J. Testud, E. Le Bouar, E. Obligis, and M. Ali-Mehenni, "The rain profiling algorithm applied to polarimetric weather radar," *J. Atmos. Ocean. Technol.*, vol. 17, no. 3, pp. 332–356, Mar. 2000.